SPi	Journal Code				Article ID				Dispatch: 10.02.16	CE:
	E	S	P		3	9	0	8	No. of Pages: 14	ME:

EARTH SURFACE PROCESSES AND LANDFORMS
Earth Surf. Process. Landforms (2016)

Published online in Wiley Online Library
(wileyonlinelibrary.com) DOI: 10.1002/esp.3908

Geomorphic influence on small glacier response to post-Little Ice Age climate warming: Julian Alps, Europe

Q1 **Renato R. Colucci***
Department of Earth System Sciences and Environmental Technologies, ISMAR-CNR, Trieste, Italy

Received 31 July 2015; Revised 18 January 2016; Revised 18 December 2015; Revised 2 December 2015; Accepted 18 January 2016

*Correspondence to: Renato R. Colucci, Department of Earth System Sciences and Environmental Technologies, ISMAR-CNR, Viale R. Gessi 2, 34123 Trieste, Italy.
E-mail: r.colucci@ts.ismar.cnr.it

ESPL
Earth Surface Processes and Landforms

ABSTRACT: The evolution of glaciers and ice patches, as well as the equilibrium-line altitude (ELA) since the Little Ice Age (LIA) maximum were investigated in the Julian Alps (south-eastern European Alps) including ice masses that were previously unreported. Twenty-three permanent *firn* and ice bodies have been recognized in the 1853 km^2 of this alpine sector, covering a total area in 2012 of 0.385 km^2, about one-fifth of the area covered during the LIA (2.350 km^2). These features were classified as very small glaciers, glacierets or ice patches, with major contribution to the mass balance from avalanches and wind-blown snow. Localized snow accumulation is also enhanced in the area due to the irregular karst topography. The ice masses in the region are at the lowest elevations of any glaciers in the Alpine Chain, and are characterized by low dynamics. The ELAs of the two major LIA glaciers (Canin and Triglav) have been established at 2275 ± 10 m and 2486 ± 10 m, respectively, by considering the reconstructed area and digital elevation model (DEM) and using an accumulation area ratio (AAR) of 0.44 ± 0.07, typical of small cirque glaciers. Changes in the ELA and glaciers extension indicate a decoupling from climate. This is most evident in the smallest avalanche-dominated ice bodies, which are currently controlled mainly by precipitation. The damming effect of moraine ridges and pronival ramparts at the snout of small ice bodies in the Julian Alps represents a further geomorphological control on the evolution of such ice masses, which seem to be resilient to recent climate warming instead of rapidly disappearing as should be expected. Copyright © 2016 John Wiley & Sons, Ltd.

KEYWORDS: ELA; LIA; avalanche; very small glacier; climate

Q2 Introduction

The first description of glaciers in the Julian Alps (southeastern European Alps) was reported in 1880 (Marinelli, 1909; Desio, 1927). Since then other researchers occasionally performed dedicated surveys, mainly concentrated in the Mount Canin area (2587 m), to characterize the geometrical evolution of the glaciers. The first surveys of Western Montasio glacier were in 1921 (Desio, 1927), while glaciological surveys began on Zeleni Sneg-Triglav glacier in 1946 (Triglav Čekada *et al.*, 2012, 2014). In total, seven glacial bodies are reported in the literature on the Italian side of the Julian Alps and one on the Slovenian side (Haeberli *et al.*, 1989).

Glaciers in the Alps attained their Little Ice Age (LIA) maximum extents in the fourteenth, seventeenth, and nineteenth centuries, with most reaching their maxima in the final AD 1850/1860 advance (Ivy-Ochs *et al.*, 2009). Wetter and cooler conditions during the nineteenth century, lead to the widespread advance of valley glaciers around 1820 and in 1850 (Orombelli and Mason, 1997). Glaciers in the Eastern Alps were smaller in 1820 than in 1850, with the Pasterze glacier, the largest valley glacier of the Austrian eastern Alps, reaching its maximum in 1850–1860 (Nicolussi and Patzelt, 2000). However, Carturan *et al.* (2014 dated [using carbon-14 (^{14}C) dating] the absolute maximum of La Mare glacier (eastern Alps) to 1600 ± 30 years. These observations mostly refer to the largest valley glaciers in the Alps, which have a greater response time compared to small cirque glaciers. Therefore, the first researchers conducting glaciological surveys in the Julian Alps likely saw the retreat of these glaciers soon after their advance 40–50 years earlier. Few glaciers persist today in the Mediterranean mountains and the majority if not all, can be considered remnants of the LIA (Hughes, 2014). In many areas the number of LIA glaciers is still unknown because research has not investigated this issue (Hughes, 2014).

The small *firn* and ice masses in the Julian Alps are considered 'very small glaciers' according to Kuhn (1995 and Cogley *et al.* (2011. Serrano *et al.* (2011 further distinguished glaciers and glacierets from ice patches of glacial and nival origin, on the basis of dynamics and genesis. Rigorous geophysical investigation may be necessary to satisfy this additional subdivision, but in most cases this paper follows this classification in the characterization of ice masses. Bahr and Radić (2012 also highlighted the importance of widespread very small ice masses because at regional scales, these features may occupy a significant volume fraction, and their omission could result

in errors of ±10%. Therefore, in the European Alps more accurate inventories of all ice bodies down to 0.01 km^2 or smaller are required to obtain evaluations with less errors (Bahr and Radić, 2012; Pfeffer *et al.*, 2014).

Very small glaciers generally experience great inter-annual mass turnover with negative or positive mass balance over the entire glacier surface (Hughes, 2008, 2010). They also respond more quickly to climate change and extremes (Hoelzle *et al.*, 2003), and may disappear or reform within a few years (Kuhn, 1995). They are commonly characterized by microclimatic conditions marginal to glacier formation, which allow them to form at a relatively low elevation, often below the theoretical regional equilibrium-line altitude (ELA, Grunewald *et al.*, 2006, González Trueba *et al.*, 2008, Hughes and Woodward, 2009). In the Dinaric Alps, the Mediterranean and the Balkans these glaciers are numerous and have recently received increased attention in order to better comprehend their behavior (Hughes, 2014). Recent work has examined the Debeli Namet in Montenegro (Hughes, 2007, 2009; Grunewald and Scheithauer, 2010; Hughes *et al.*, 2011; Djurovič, 2012), very small maritime glaciers of the Prokletjie mountain in Albania (Milivojevič *et al.*, 2008; Hughes, 2009), the Snezhnika glacier in the Bulgarian Pirin mountains (Grunewald and Scheithauer, 2010), the Skuta glacier in the Kamnik-Savinja Alps of Slovenia (Šifrer and Košir, 1976; Triglav Čekada *et al.*, 2012), very small niche glaciers and permanent snow fields in the Mount Olympus in Greece (Styllas *et al.*, 2015) and the Calderone glacier in the Italian Appenines (e.g. Gellatly *et al.*, 1994; D'Orefice *et al.*, 2000; Pecci *et al.*, 2008). Despite a relatively well-documented recent history of glaciers, very little is known about conditions during the LIA, although in some areas it has been reported that glaciers in the late nineteenth century were some of the biggest during the entire Holocene (Hughes, 2014).

Commonly in the literature, the only modern or recent glacier reported from the Julian Alps is a very small glacier below the Slovenian peak of Triglav (e.g. Hughes *et al.*, 2006; Grunewald and Scheithauer, 2010; Hughes, 2010; Djurovič, 2012; Hughes, 2014). Additional very small glaciers in the region, about 30 km west of Triglav, have been investigated in detail recently (Carturan *et al.*, 2013; Triglav Čekada *et al.*, 2014; Colucci and Guglielmin, 2015; Colucci *et al.*, 2015). These glaciers are all located in the same climatic area, characterized by some of the highest precipitation rates in the European Alps. An investigation of these features presents an opportunity for a better comprehension of the recent, past and future evolution of small glaciers, not only in this region but also at a broader scale.

This paper aims to: (1) investigate the glacial evidence of Julian Alps (south-eastern European Alps) since the LIA, taking into account minor ice masses, which have previously been overlooked; (2) estimate the reduction in glacier area since the LIA maximum up to the present day (2012); (3) estimate the regional ELA evolution since the LIA maximum up to the present.

Study Area

The Julian Alps occupy 1853 km^2, spanning west to east across the Italian–Slovenian border (Figure 1). The mountain range is characterized by carbonate massifs, reaching the highest elevations at Mount Triglav (2864 m), Mount Montasio (2754 m) and the Mount Škrlatica (2740 m, see Figure 1). The bedrock consists of Upper Triassic carbonate succession of dolostone (Dolomia Principale) and limestone (Dachstein Limestone), and glaciokarst landscape is widespread (*sensu* Žebre and Stepišnik, 2015). The drainage divide between the Adriatic Sea and the Black Sea crosses Julian Alps in the range of the Mount Canin (2587 m). The 1981–2010 climatology at 2200 m above sea level (a.s.l.) in this area has recently been reconstructed by Colucci and Guglielmin, (2015). Mean annual precipitation (MAP) is estimated at 3335 mm w.e. February is the driest month (180 mm w.e.) and November the wettest (460 mm w.e.). Mean annual air temperature (MAAT) is 1.1 ± 0.6 °C. Temperatures in February are the lowest (−6.0 ± 2.9 °C) while the highest are recorded in July (9.2 ± 1.3 °C). Average winter snow accumulation (C_w) of 6.80 m was measured between December and April at 1830 m a.s.l. Over the same period, MAAT measured at the Kredarica observatory of Mount Triglav (2547 m) was −1.0 ± 0.6 °C with February being the coldest month (−8.1 ± 2.9 °C) and July the warmest (6.9 ± 1.3 °C), and MAP 2071 mm w.e.

Methods

The Julian Alps area was investigated in the field between 2011 and 2014, typically in late summer and early autumn when snow cover was at its minimum. The area of Canin was also surveyed in 2011 and 2013 with a dedicated airborne laser scanning (LiDAR, light detection and ranging) at the end of the ablation season in late September.

Glacier-covered areas of 2012 were also identified using Bing maps (www.bing.com/maps/). The images were acquired after a hot and dry summer that followed a very dry winter so little scattered residual snow cover was present and *firn* and ice surfaces were well exposed. The imagery was georeferenced with an image-to-image registration method. A 2006 digital elevation model (DEM) derived from a 1 m × 1 m cell LiDAR, in conjunction with high resolution orthophotos, were used to select the ground control points for the georeferencing (e.g. Brook *et al.*, 2011). The absolute error associated with this methodology is about ±25 m^2 (Fitzharris *et al.*, 1997). Orthophoto of the Slovenian Julian Alps from the ARSO Geoportal (http://gis.arso.gov.si/geoportal/catalog/) were loaded into a geographic information system (GIS) using the same approach with a 12.5 m × 12.5 m cell DEM. The surface areas of Canin and Ursic glaciers in 1908 were inferred by georeferencing the original map drawn by Marinelli (1909. Glacier surface areas for Triglav are from Triglav Čekada *et al.* (2014) and Gabrovec *et al.* (2014).

The LIA glacier limits were reconstructed based on geomorphological mapping conducted on the field, the analysis of LiDAR, aerial photographs, orthophotos and archival pictures and maps. The margins of former ice bodies were easily identified due to well-preserved frontal and lateral moraines and pronival ramparts. The identification of upper headwall limits of ice during the maximum LIA extent was possible due to the persistence of trimlines, recognizable from the clear difference in bedrock color (Figure 2a).

Landforms (moraines and ridges, suffosion dolines, debris flows) were added to 1:5000 base maps by using 1 m × 1 m LiDAR imagery and/or a set of high resolution (0.15 × 0.15 m px^{-1}) orthophotos.

A simple degree-day model was used to calculate the snow accumulation (in mm w.e.) required to sustain the present glaciation in the Julian Alps (Hughes, 2010). The 1981–2010 mean daily air temperatures (MdATs) at 2200 m a.s.l. from Colucci and Guglielmin (2015 were averaged to obtain an annual daily temperature curve. The 1981–2010 MdAT was extrapolated to the median elevations of all the glacial bodies using a normal lapse rate of 0.0065 °C m^{-1}. The median

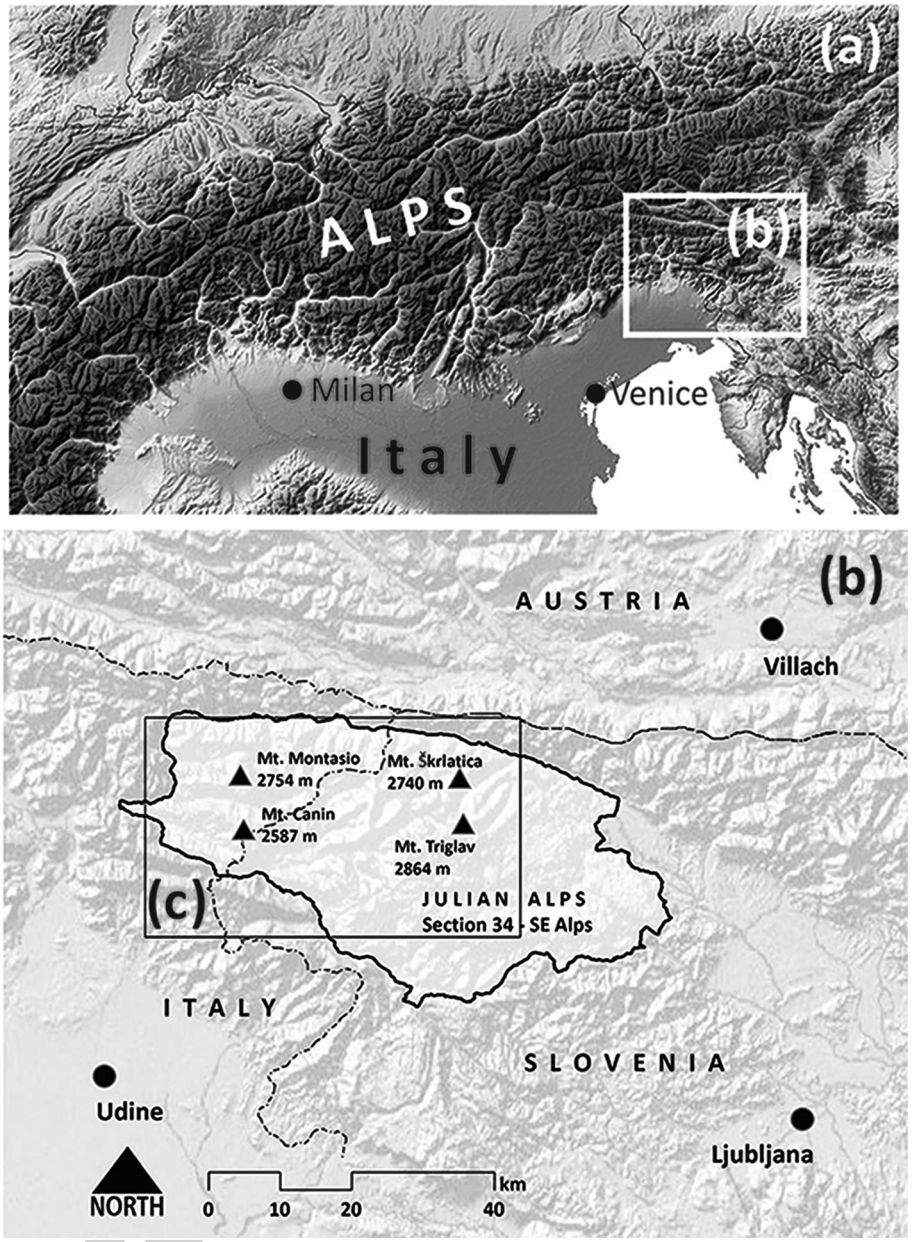

Figure 1. Study area with the location of: (a) the Alpine Chain, courtesy of Scilands GmbH; (b) the Julian Alps; (c) the section of Julian Alps used for Figure 3.

elevation of each ice body was extrapolated from the DEM according to Braithwaite and Müller (1980.

Next, the annual accumulation required to balance melting at each glacier, was calculated using a degree-day factor of 4.1 mm day^{-1} K^{-1} ± 1.5 mm day^{-1} K^{-1} (standard deviation 2σ: ±36%) which is representative of most glaciers (Braithwaite, 2008).

Commonly, greater winter precipitation accumulates in cirques due to windblown deposition and avalanche compared to plateau glaciers (Dahl and Nesje, 1992). The contribution from avalanches was calculated according to Hughes (2008, 2010 by determining the avalanche ratio (V/A), where V is the total area susceptible to avalanche and A is the total glacier area. The value of V was defined as the area with slope $> 30°$ leading directly onto the glacier accumulation area. The avalanche ratio was calculated for both the LIA and present day (Table I).

Glacier volume was estimated using an empirical volume–area relation widely applied in glacier inventories and water resources estimation, based on data from 144 mountain glaciers, using Equation 1 from Bahr *et al.* (1997) and Bahr *et al.* (2015 where S represents the glacier surface:

$$V = 0.03\ S^{1.36} \tag{1}$$

Glacier surface areas during the LIA were inferred from geomorphological evidence and drawn in a GIS. Upper surfaces were assumed to have concave ice contours, while the lower surfaces were convex. The LIA ELA was estimated using an AAR of 0.44 ± 0.07, which is considered the most appropriate value for glaciers in the range of 0.1 to 1.0 km^2 (Kern and László, 2010). The calculation was automated using a GIS tool developed by Pellitero *et al.* (2015 and only used for Canin and Triglav glaciers, which, due to their size, both better reflected the relation with climate during the LIA.

The evolution of the ELA in the twentieth century was reconstructed using a best-fit relation between summer air temperature (T_{sum}) and total annual precipitation (P_a) at the ELA. This reconstruction was only determined for Canin glacier, which

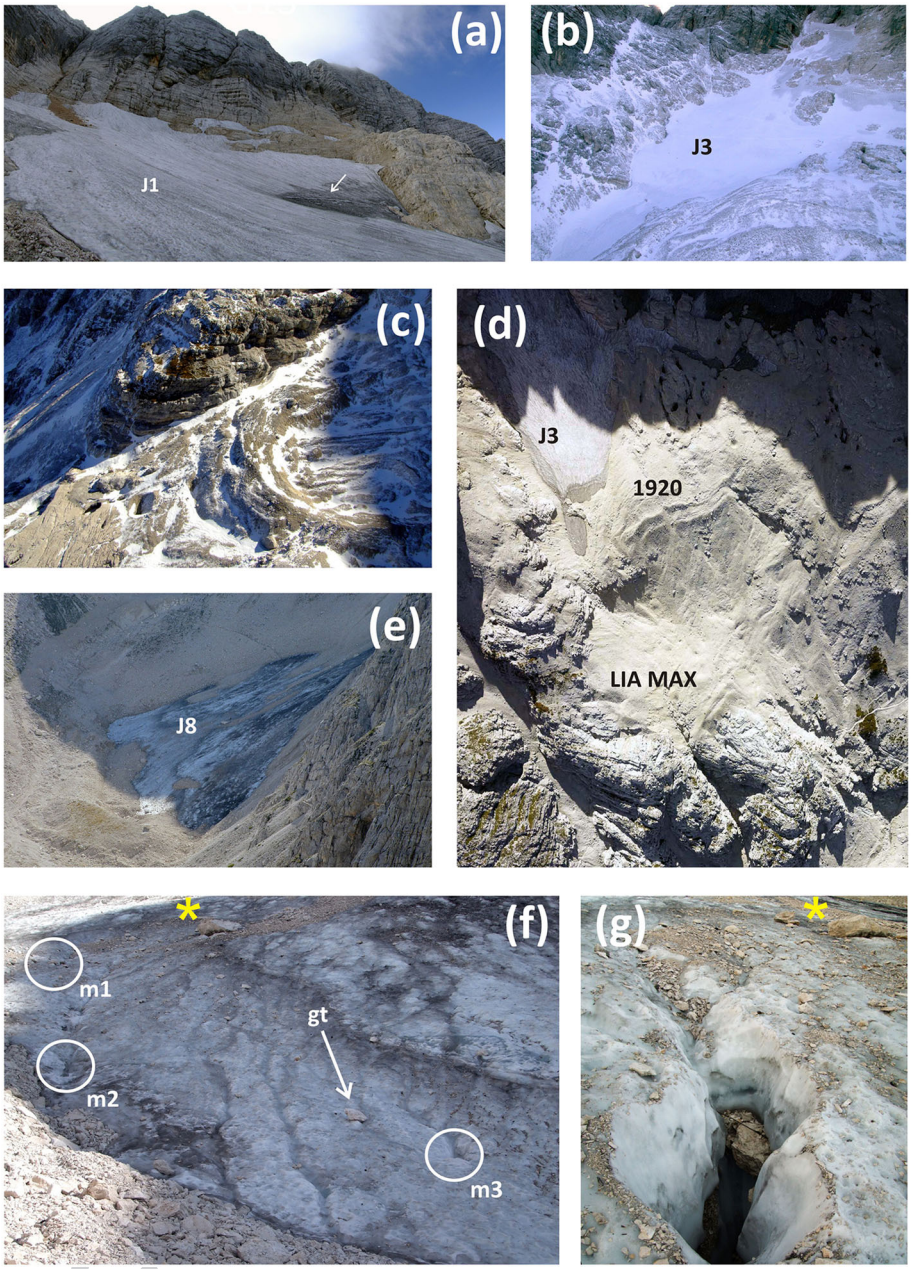

Figure 2. (a) Photograph of Canin West 1 (J1) with the very evident trimline identifiable by the change in color of Dachstein limestone; the arrow indicates a small crevasse. (b) Canin East (J3) as seen in late October 2014 from the helicopter; maximum length is about 300 m. (c) Little Ice Age (LIA) frontal moraines (maximum width is 77 m) of the Canin glacier as seen in late October 2014 from the helicopter. Note some fluted moraines partially shaded on the right of the photograph. (d) The lower part of Canin East glacieret (orthophoto; October 4, 2013) with the evidence of 1920 and LIA MAX moraines, whose maximum distance is about 220 m. (e) Prevala glacieret (J8) as seen from the Gilberti hut (see Figure 1 for location); in the down-left side of the picture the sun highlights the two frontal moraine ridges; (f) The front of Prevala glacier in late August 2012. Is evidence of the network of supra-glacial streams some of them terminating in the moulins highlighted by circles; gt arrow indicates a glacier table formed by differential melting. (g) The entrance of the 4 m deep active moulin m1. For scale, moulin m1 and m3 are located about 90 m from each other.

had the longest available record. The value of T_{sum} was solved using the 1920–2012 P_a in Equation 2 (Ohmura *et al.*, 1992):

$$P_a = 645 + 296\ T_{sum} + 9\ T_{sum}{}^2 \quad (2)$$

The calculation was performed for each year and the annual T_{sum} at the ELA was obtained at the 'right' elevation. The reconstructed monthly temperature at 2200 m from Colucci and Guglielmin (2015 was used, with a normal lapse rate of 0.0065 °C m^{-1}. The standard error of Equation 2 is ±200 mm, so the calculation was performed using both extremes to determine the standard error in T_{sum} and, as consequence, the ELA error.

Results

Glaciers in the Julian Alps

There is evidence of 23 permanent ice patches and glacierets in the Julian Alps (Figure 3), covering a total area of **F3** Q7 0.385 km^2 (Table I) and having an estimated volume of 0.003 km^3. All features have a northerly aspect, and have developed at the base of steep rock slopes that favor avalanche activity, windblown snow deposition and summer shading. The Western Montasio (0.07 km^2) is the largest, followed by the Canin West 2 and 1 (0.023 km^2 and 0.019 km^2) and the Canin East (0.014 km^2). Three other snow patches with westerly

or southeasterly aspects have been recognized in the area, but are only able to persist during periods of high winter precipitation and cool summers and are thus semi-permanent (Figure 3).

Canin-Cergnala

At present (2012), six ice patches and glacierets occupy the area of the former Canin glacier. Several minor glacial ice patches, generally located in karst depressions, persist in favorable microclimates. The glacial ice patches of Canin West 1 and 2 have concave-down profiles and the ice surface is characterized by a series of dark bands, likely related to ice movement from rotational slipping. The Canin East has a subdued concave-up profile and a series of irregularly-spaced convex bands of fine, sediment-rich ice over the surface. These features are interpreted to have formed from variations in ice/*firn* velocity across the glacieret, and hint at present dynamics (Colucci and Guglielmin, 2015). In October 2011, ground penetrating radar (GPR) indicated an average glacier thickness of 11.7 m, and the volume was calculated at 205 000 m^3 (Colucci *et al.*, 2015). A system of well-developed frontal moraine ridges outlines the LIA maximum of Canin and Ursic glaciers (Figures 2c, 2d and 4a). Moreover, the inferred extent of Canin glacier in 1908, roughly overlap two parallel moraine crests located 25 to 200 m south of the LIA terminus (Figure 4a), which may indicate the 1910–1920 advance (Desio, 1927). Further north, several fluted moraines are located on the western portion of the former Canin glacier, indicating higher dynamics controlled by topography (Figures 2c and 4a). The morainic material is often studded with suffosion dolines, with diameters ranging from 10 to 50 m and from a few meters up to 15 m thick (Figure 4a). Outcropping polished surfaces and *roche moutonée* display several striae and sub-glacially precipitated carbonate crusts typical of basal sliding in warm-based glaciers (Refsnider *et al.*, 2012). Their appearance and preservation suggest limited exposure to chemical weathering (Hughes, 2007). A trimline is apparent over the back rock slope, identifiable as a change in the rock color (Figure 2a). Lateral moraines are also well preserved, particularly on the right side of the glacier. During the peak of the LIA, Canin glacier was likely connected to Ursic glacier (Marinelli, 1909; Colucci *et al.*, 2015), forming a unique ice mass with a reconstructed area of 0.85 km^2. Evidence of permanent nival ice patches exists on the south-eastern side of Canin, where small glaciers may have developed during the LIA (Figure 3). In these areas, widespread snowfields recently survived through summer 2009 and 2014 (Colucci *et al.*, 2014b).

Ursic glacier, which still persisted in 1988 (Haeberli *et al.*, 1989), melted during the 1990s and now only a few permanent snow/*firn* patches remain in its stead. The well-preserved frontal morainic system from the LIA maximum is characterized by breach-lobe moraines. These features are typical of glaciers with low dynamics that grow more in thickness (volume) than in area (e.g. Žebre and Stepišnik, 2015). The presence of buried ice below the debris is possible, but this was not investigated. East of Ursic, a very small permanent ice body fed by avalanches lies at the bottom of the steep rock walls of the Cima Gilberti (2417 m), shaded for most of the year.

The Prestrelienik glacier, still existing in 1985 (Haeberli *et al.*, 1989), was thought to have melted, but a GPR survey (unpublished data) in summer 2014 identified ice >10 m thick buried by debris and snow/*firn* layers. The *firn* was in contact with the most internal moraine ridge. This ridge likely formed during the 1910–1920 advance of the Canin glacier, while the lower subparallel morainic ridges are likely associated with the LIA maximum.

Surprisingly, the very small Prevala glacier (Figures 2e–2g) was previously classified as a permanent snow-field (Tintor, 1993). There was no mention of this ice body in the literature, which is still in contact with its frontal moraine. GPR surveys of the feature from 2011 and 2013 identified the presence of a 5 to 20 m thick layer of ice under a 10 to 15 m of snow and *firn* (Forte *et al.*, 2014a, 2014b). The glacier is about 300 m long, a maximum of 100 m wide, and covers an area of 0.051 km^2, lying between 1826 m and 1941 m a.s.l. During late summer 2012, after a very dry winter, the ice of Prevala was exposed over almost the entire glacier surface. Transversal cracks 1 to 2 cm wide and several tens of meters long were observed, with fault planes formed by thrust faulting. This is consistent with a basal shear stress sufficiently high to encourage basal sliding. A complex system of *bedières* and two small active moulins, up to 4 m in depth, drain surficial meltwater (Figures 2f and 2g). The visible stratigraphy in the moulins revealed alternating layers of debris and *firn*. At the snout of Prevala there are two parallel ridges close together (Figures 2e and 4b), mainly composed of clast-supported, poorly sorted sub-angular clasts. However a few sub-rounded clasts are present, especially in the outermost ridge. Several boulders are present both within and on top of the crests, with the largest having an *a*-axis > 3 m. A lower percentage of angular clasts is also present, suggesting coupled glacial-avalanche transport of the debris. The high *V/A* ratio (Table I) allows this very small glacier to persist under present climate conditions. Together with the Western Montasio, the Prevala represents the lowest documented glacial evidence on the southern side of the European Alps.

Two other previously unreported permanent ice patches are the Vasto and the Cergnala. The first developed in a narrow incision, and a 2012 GPR survey indicated the presence of ice >15 m thick and internal layering with upward concavity sloping towards the front (Colucci *et al.*, 2014a). Almasio (2002 first reported the feature and also recognized a small morainic ridge at its snout. The Cergnala is an avalanche-fed nival ice patch 200 m long and 50 m wide. Scattered perched blocks, some with an *a*-axis > 3 m, are located around its snout. These outline the present ice patch boundary and other likely more extensive phases. Further discussion is difficult due to the lack of a clear morainic ridge or signs of present dynamics.

Montasio-Jof Fuart

In the Montasio and Jof Fuart areas, five ice bodies have been mapped: three in the Montasio area and two in Jof Fuart.

The Western Montasio is a cone-shaped, avalanche-fed small glacier with an area of 0.07 km^2. Carturan *et al.* (2013 recently investigated the glacier, and in 2011 its average thickness and volume were estimated at 15 m and ~1.0 $\pm 10^6$ m^3 respectively. Two parallel ridges about 400 m from the back wall form the frontal moraine complex, with the inner one ascribed to the beginning of the twentieth century and the larger outer ridge to the LIA maximum. Lateral moraine remnants are visible on the right flank of the glacier, and the frontal moraine is still in contact with the ice body. The glacier front is buried by a thick debris cover that allowed the measurement of a radial patterned surface average velocity of 19 cm $yr.^{-1}$ in 2011.

The smaller Eastern and Minor Montasio ice patches are well documented in the literature (Rabagliati and Serandrei Barbero, 1982; Haeberli *et al.*, 1989; Serandrei Barbero *et al.*, 1989). These two features are situated a few hundred meters east of the Western Montasio, at about the same elevation (Figure 5 b). A series of irregularly-shaped pronival ramparts with very angular to angular clasts are present at their fronts. This is consistent with a snow-avalanche dominated development process for such features (Matthews *et al.*, 2011), rather than for

Q4 **Table I.** Present (2012) and Little Ice Age (LIA) maximum extent of the permanent SFB of Julian Alps. Equilibrium-line altitude (ELA) of the LIA maximum is also reported (AAR 0.44) together with present and LIA *V/A* for each SFB

					2012						
ID	Name	WGI	ID WGMS	CGI	Area (km^2)			a	b	c	d
J1	Canin West 1		680	985	0.019	0.076	0.083	2286	2254	2359	0.5
J2	Canin West 2	IT4L00003004		985.1	0.023			2307	2275	2375	0.4
	Canin West patches			—	0.008			2234	2223	2257	0.9
J3	Canin East 1	IT4L00003002	640	984	0.014			2169	2147	2228	1.3
	Canin East patches			984.1	0.012			2223	2203	2243	1.0
J4	Vasto	—	—	—	0.001			2199	2188	2246	1.1
J5	Ursic	IT4L00003003	2652	983	0.003	0.006		2252	2242	2264	0.8
J6	Torre Gilberti	—	—	—	0.003			2204	2193	2224	1.1
J7	Prestrelienik	IT4L00003006	—	982	0.020			2127	2112	2162	1.6
J8	Prevala	—	—	982.1	0.012			1862	1826	1941	3.3
J9	Cergnala	—	—	—	0.011			1942	1919	1978	2.8
J10	Montasio West	IT4L00003005	641	981	0.071			1906	1859	2090	3.0
J11	Montasio East	IT4L00003001	1121	980	0.038			1895	1823	1947	3.1
J12	Montasio Minor	IT4L00003006	—	979	0.004			1815	1801	1850	3.6
J13	Studence	—	—	—	0.008			1829	1811	1859	3.5
J14	Carnizza-Riofreddo	—	—	—	0.019			1750	1697	1849	4.0
J15	Bavski Grintavec	—	—	—	0.021			2001	1981	2101	2.3
J16	Zeleni Sneg - Triglav	—	3662	—	0.006			2451	2402	2516	-
J17	Triglav minor	—	—	—	0.001			2672	2655	2697	-
J18	Krnica	—	—	—	0.029			1962	1911	2098	2.6
J19	Ponca North	—	—	—	0.008			2274	2225	2420	0.8
J20	Ponca East	—	—	—	0.028			2247	2140	2481	0.7
J21	Low Oltar	—	—	—	0.008			2051	2020	2082	2.0
J22	High Oltar	—	—	—	0.015			2280	2237	2390	0.5
J23	Dovski Kriz	—	—	—	0.003			2253	2200	2342	0.7
	JULIAN ALPS				**0.385**						

moraines of glacial origin. The presence of sub-angular clasts also suggests a coupled mechanism for the genesis of the ridges, especially in the central part of the complex of Eastern Montasio located about 140 m from the slope break at the cliff face. Gaps and gullies that act as avalanche routes have formed between the pronival ramparts. These are also evident due to the scoured bedrock headwalls along the avalanche paths and the presence of debris fans in the run-out zones.

Two other unreported permanent ice patches similar to Eastern and Minor Montasio have been recognized at the foot of the steep rockwall of Mount Jof Fuart (2666 m): the Studence (Figure 5a) and the Rio Freddo (Figure 5d). These features, respectively, have north-western and northern aspects and are bounded by irregularly-shaped ridges. The frontal ridges are composed mainly of angular to very angular clasts. Nevertheless, the presence of some sub-angular clasts indicates a glacial mechanism in their development. The maximum distance from their ridges to their back cliffs exceeds 180 and 140 m, respectively. Some *bergschrund* are present in the apical area mainly due to the high of the narrow gorges in which they are located.

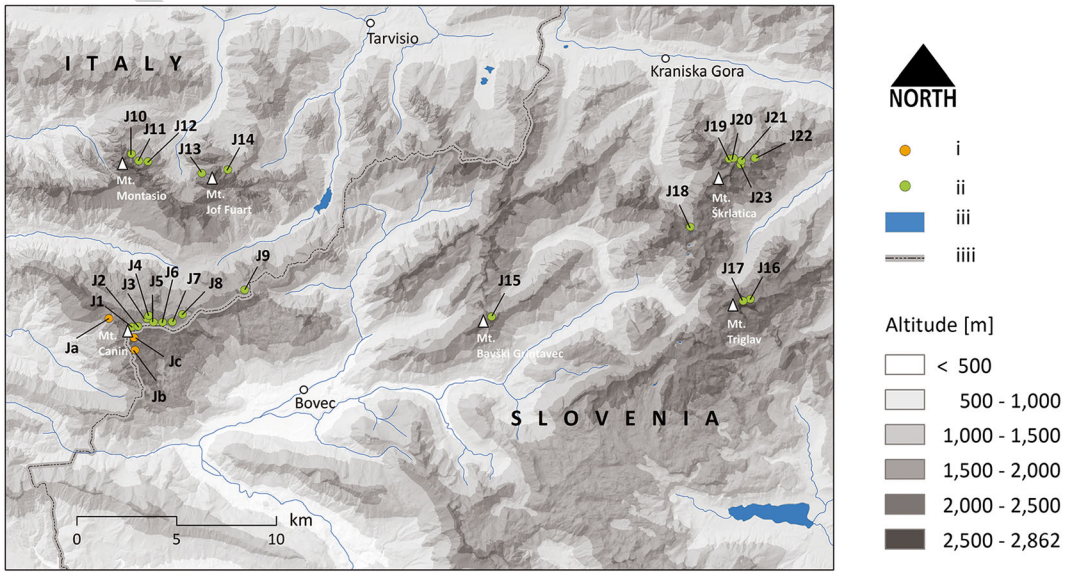

Figure 3. Location map of the permanent SFBs of the Julian Alps, (b) in Figure 1. See Table I for name of features: (i) semi-permanent SFBs; (ii) permanent SFBs; (iii) lakes; (iiii) border (Italy– Slovenia).

Table I. Present (2012) and Little Ice Age (LIA) maximum extent of the permanent SFB of Julian Alps. Equilibrium-line altitude (ELA) of the LIA maximum is also reported (AAR 0.44) together with present and LIA *V/A* for each SFB

	2012		1908	LIA Max						area 2012 versus			
ID	e	f	Area (km^2)	Area (km^2)		g	h	i	ELA AAR 0.44	area LIA Max		*V/A* 2012	*V/A* LIA
J1	4161	1576	0.427	0.672	0.853	2251	2059	2476	2275 ± 10	0.113	0.124	1.7	0.9
J2	4084	1576										1.6	
	4475	1576										—	
J3	4794	1576										3.0	
	4555	1576										—	
J4	4634	1576		0.001					—	1.000		2.0	
J5	4396	1576	0.085	0.181					2269 ± 10	0.033		6.0	1.4
J6	4634	1576										6.7	
J7	5037	1576		0.275		2207	2072	2379	2235 ± 10	0.073		9.3	1.0
J8	6473	1576	—	0.051		—	—	—	—	0.235		9.0	2.2
J9	6037	1576	—	0.129		—	—	—	—	0.085		3.9	1.1
J10	6209	1576	—	0.099		—	—	—	—	0.717		2.5	1.8
J11	6297	1576	—	0.064		—	—	—	—	0.594		5.0	2.9
J12	6743	1576	—	0.008		—	—	—	—	0.500		8.1	3.8
J13	6652	1576	—	0.019		—	—	—	-	0.421		17.5	8.1
J14	7120	1576	—	0.060		—	—	—	—	0.317		7.8	3.3
J15	5553	1576	—	0.050		—	—	—	—	0.420		1.5	1.0
J16	3269	790	—	0.404		2458	2268	2630	2486 ± 10	0.015		—	0.8
J17	2324	790	—	0.035		—	—	—	—	0.029		—	—
J18	5808	790	—	0.079		—	—	—	—	0.367		2.9	1.1
J19	4201	790		0.018		—	—	—	—	0.444		4.2	2.9
J20	4257	790	—	0.059		—	—	—	—	0.475		2.1	1.4
J21	5302	790	—	0.023		—	—	—	—	0.348		5.4	1.9
J22	4101	790	—	0.040		—	—	—	—	0.375		6.2	2.3
J23	4257	790	—	0.074		—	—	—	—	0.041		19.0	1.3
				2.341						**0.164**			

[a]Note: WGI, ID WGMS and CGI indicate respectively the World Glacier Monitoring Inventory ID (http://nsidc.org/data/glacier_inventory/browse.html), the World Glacier Monitoring Service Database ID (http://www.wgms.ch/metadatabrowser.html), and the CGI and EVK2-CNR inventory ID (http://users.unimi.it/glaciol/). (a) 2012 median elevation (in meters); (b) 2012 minimum elevation (in meters); (c) 2012 maximum elevation (in meters); (d) 1981–2010 mean annual air temperature (MAAT) at altitude a); (e) annual accumulation (in mm w.e.) required to balance melting; (f) 1981–2010 mean winter precipitation (November–April); (g) LIA media elevation (in meters); (h) LIA minimum elevation (in meters); (i) LIA maximum elevation (in meters). Q5

Triglav-Bavški Grintavec

Two glaciers in the Slovenian sector of the Julian Alps have been reported in the literature: The Zeleni Sneg-Triglav and the Bavški Grintavec. The Zeleni Sneg-Triglav (Figure 6a) is F6 an ice patch of glacial origin with a northeast aspect, and lies between 2400 and 2500 m (Gabrovec *et al.*, 2013). In 2012, the total area determined from LiDAR was 0.006 km^2 (Triglav Čekada *et al.*, 2014) but during the LIA the glacier covered an area of about 0.4 km^2 (Šifrer, 1963; Gabrovec *et al.*, 2014). There is documented evidence of an advance in the 1920s, when the glacier was larger than in previous years (Gams, 1994). At present the glacier has almost completely melted away and the dramatic decrease in area and volume was particularly evident during the 1980s and 1990s. In autumn 2013, a GPR survey indicated a basal ice layer that averaged 1.95 m thick, below a 1 to 2 m layer of snow and *firn* (unpublished data). Below the peak of Bavški-Grintavec (2344 m) some permanent, avalanche-fed snow patches are present, but until the 1980s the cirque was partially filled by *firn* and ice (Tintor, 1993). The snow patches currently occupy an area of 0.018 km^2, but during the LIA maximum there was a small glacier with a reconstructed area of 0.050 km^2 (Figure 6d). The glacier rapidly melted away over the past decades due to the low elevation and the *V/A* ratio. The presence of buried ice below the debris is possible, but this was not investigated. The cirque has a frontal moraine ridge with large boulders on the main crest near its edge.

Škrlatica-Dovški Križ

There is evidence of six permanent ice patches in the Škrlatica massif. The Ponca North and Ponca East are two avalanche-fed ice patches located under the Velika Ponca peak (2602 m) (Figures 5c and 6c). The shape of Ponca North is largely a result of the intense avalanche activity induced by the steep and high rock wall of Velika Ponca. Ponca North is mostly within a 250 m long gully cut into the cliff face, and some *bergschrund* are visible in the uppermost area. Large avalanches canalize almost from the top of the rock wall to the vast scree slope at its base. Two prominent sediment ridges extend beyond the ice patch, the western measuring 310 m and the eastern 420 m long. These two ridges become closer together about 200 m from the back cliff. Here an internal (frontal) ridge appears cut by avalanche routes and debris flows, so snow and sediments are presently transported up to 500 m downhill from the wide apex of the ice patch in its central part, where a *bergschrund* was observed in 2012.

The Ponca East, at the same elevation, is more shaded due to its northerly aspect. The feature is bordered by a sub-parallel sedimentary ridge 50 m from the rear cliff. Debris flow routes cut the ridge to the northeast where the slope is greater.

Some permanent snow patches exist in two cirques below the peaks of Veliki Oltar (2628 m) and Dovški Križ (2542 m). These patches are presently only able to persist in shaded, north-facing areas. The patches are fed by avalanches and windblown snow, processes that were likely crucial in

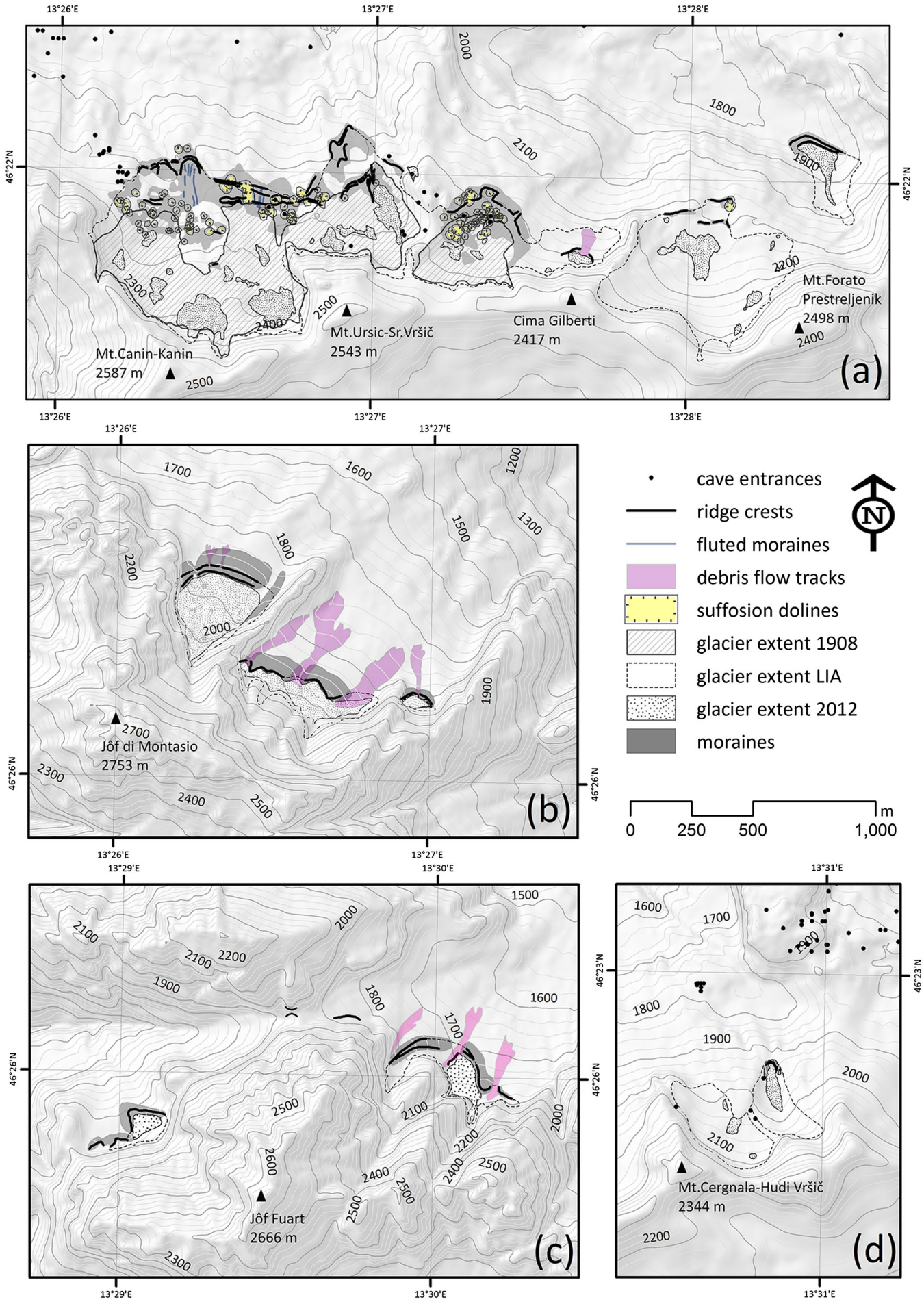

Figure 4. Glacio-geomoprhological maps of the Italian sector of Julian Alps: (a) Canin; (b) Montasio; (c) Jof Fuart; (d) Cergnala.

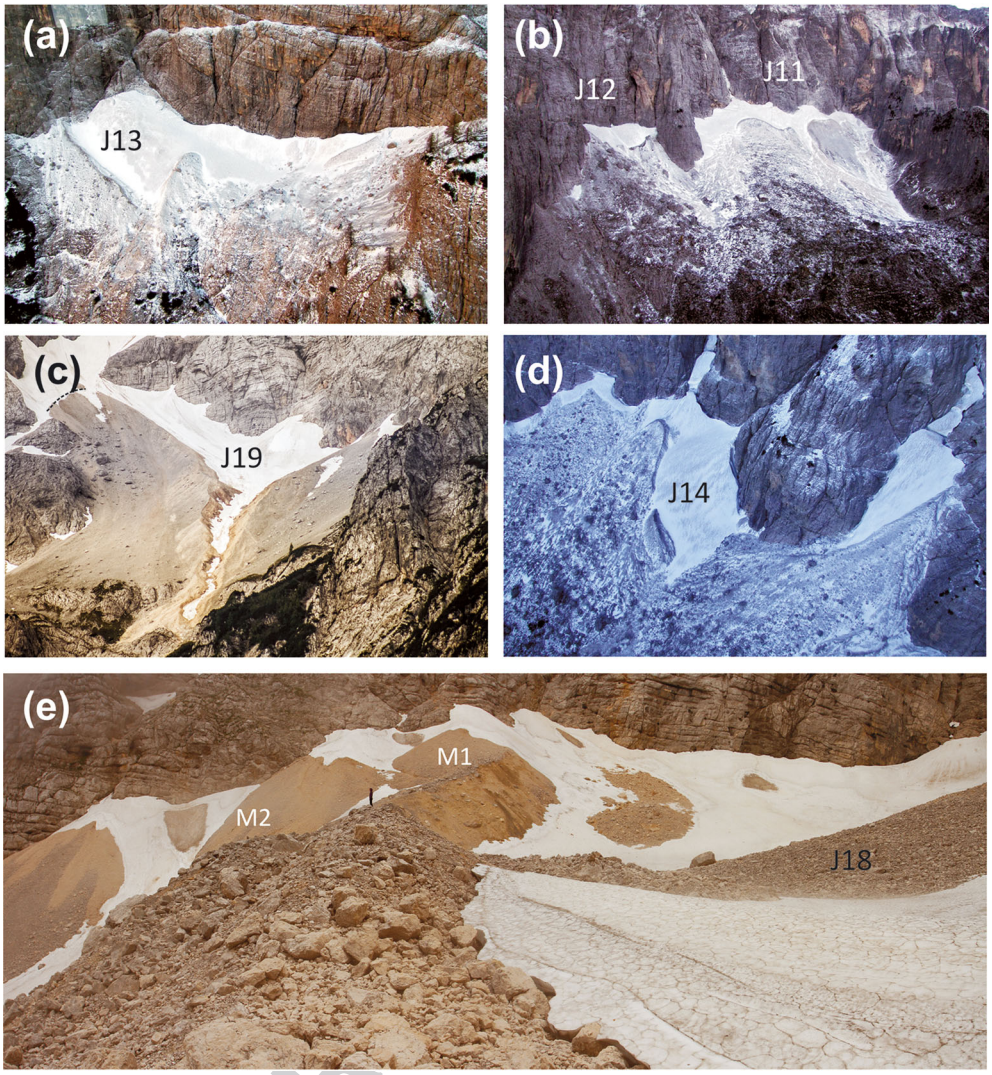

Figure 5. Some of the ice bodies in the Montasio-Jof Fuart and Škrlatica sectors: (a) Studence (J13), about 240 m wide; (b) Montasio Minor and Montasio East (J12–J11), the latter being about 570 m wide; (c) Ponca North (J19); (d) Rio Freddo (J14) with its frontal ridge lying about 140 m from the back cliff; (e) the two sub-parallel and juxtaposed frontal 10 moraine ridges (M1 and M2) of Krnica SFB (J18). See person on moraine M1 for scale and note the important topographic difference inside (right) and outside (left) the moraine complex.

preserving small glaciers during the LIA. Frontal moraines lie at the edge of both cirques; at Veliki Oltar the moraine is particularly high and well preserved. The moraines are located at *c.* 2225 and 2200 m elevation, respectively, about 150 m higher than the LIA Canin moraine complex and roughly 100 m lower than the LIA maximum moraine complex of Triglav. Future geophysical investigations will determine whether buried ice from the LIA has survived below the debris. Another small avalanche-fed ice patch persists at relatively low elevation in the Low Oltar sector due to its high *V/A* ratio. The feature is bounded by a lobate sedimentary ridge up to 120 m away from the rear cliff. Two debris flow/avalanche routes cut the ridge near its center.

Further south, in the upper Krnica valley, an ice patch is located in a narrow cirque characterized by high and steep walls, which favor avalanche feeding and summer shading (Figure 6b). The ice patch has a significant debris cover and partially overlying *firn* and ice deposits. The snow and *firn* patches have a mean elevation of 1962 m and cover 0.029 km^2, 37% of the estimated LIA maximum extent. Two sub-parallel and juxtaposed frontal moraine ridges (Figure 5e) are well-preserved and have been described by Kunaver (1999 as the result of the last stage of the glacier. A third smaller ridge is located in the inner part of it. The moraines are composed of clast-supported sediments with sub-angular clasts. The lack of soil development suggests recent surface exposure, indicating that the moraine complex is associated with the LIA maximum. The innermost ridge may also have formed during the 1910–1920 phase like the features in the Canin-Cergnala and Montasio-Jof Fuart sectors. The topographic relief of the moraine complex is remarkable, which may indicate the presence of thick, debris-rich ice deposits (Figure 5e).

At present (2012), a total of 0.385 km^2 of the Julian Alps is covered by glacial features.

ELA reconstruction and evolution

The ELA was calculated based on the reconstructed area and DEM of Canin and Triglav glaciers (Figure 7). ELAs of 2275 ± 10 m for Canin and 2486 ± 10 m for Triglav were determined with an AAR of 0.44 ± 0.07 (Kern and László, 2010); lower ELAs of 2225 m and 2436 m were obtained using an AAR of 0.67 (Gross *et al.*, 1977; Braithwaite and Müller, 1980). The median glacier elevations derived from the reconstructed LIA DEMs were 2251 m for Canin and 2448 m for Triglav. **F7**

The historic record of variation in the Canin East glacier front was used to compare the 11-year running mean record of ELA. Figure 8 shows that the two records are generally anti-correlated, i.e. that the glacier front was advanced when the **F8**

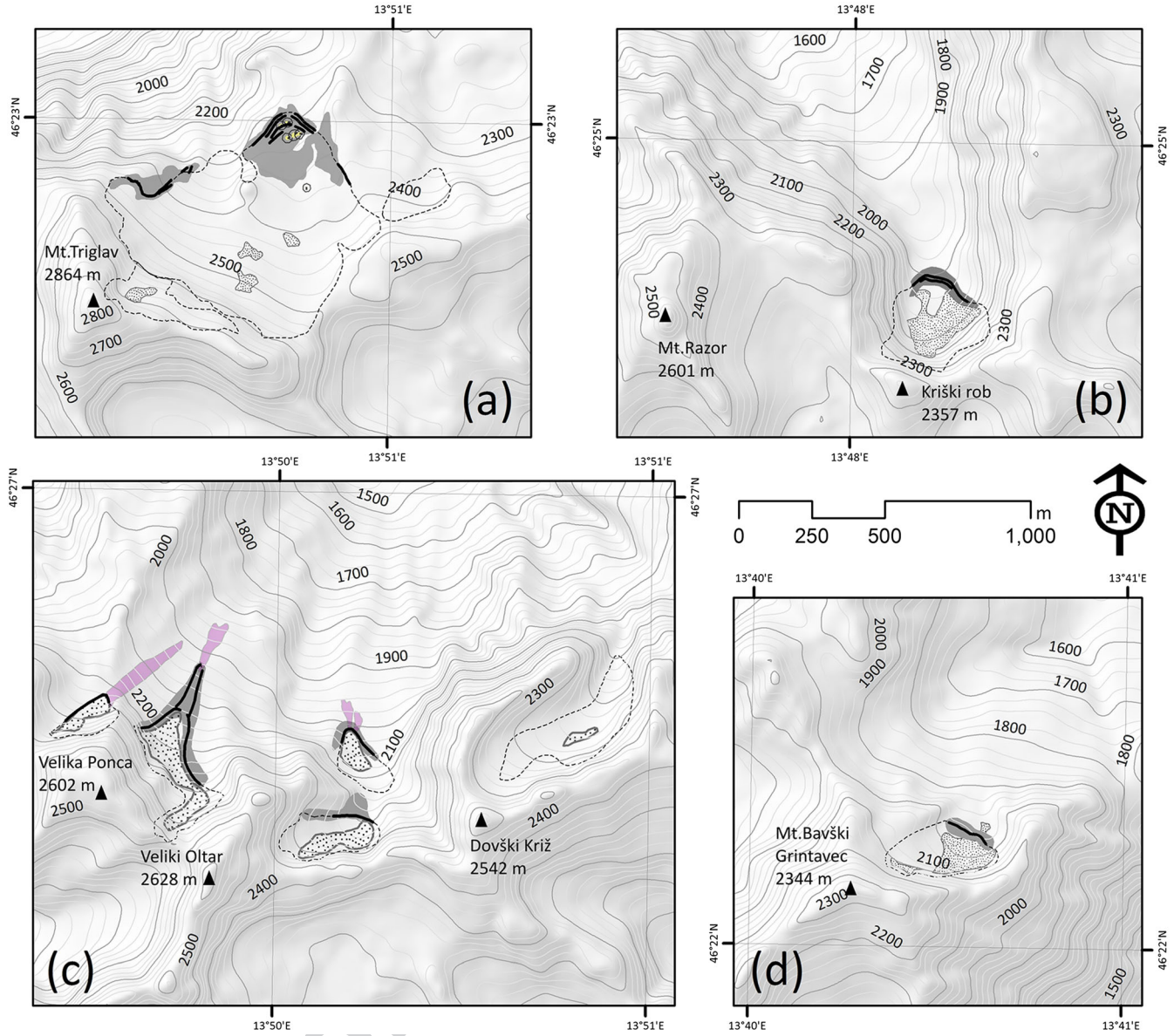

Figure 6. Glacio-geomorphological maps of the Slovenian sector of Julian Alps: (a) Triglav; (b) Bavski Grintavec; (c) from left to right Ponca East, Ponca North, High Oltar and Low Oltar, Dovški Križ; (d) Krnica.

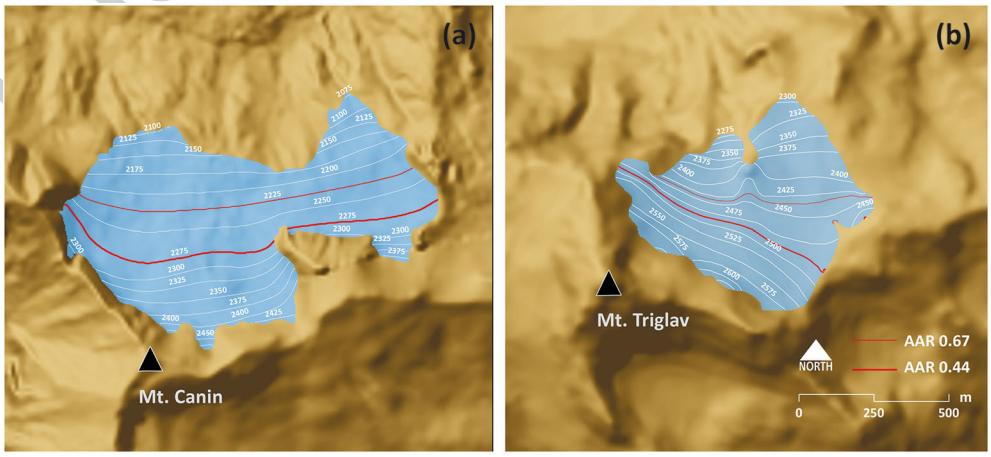

Figure 7. Visualization of the equilibrium-line altitude (ELA) accumulation area ratio (AAR) applied with both 0.44 and 0.67 AAR: (a) LIA Canin glacier; (b) LIA Triglav glacier.

ELA was lower, and vice versa. During the documented Canin glacier advance in the 1920s that formed a secondary moraine complex, reconstructed ELA was between 2280 and 2350 m, roughly 40 m higher than the reconstructed ELA during the LIA maximum when the glacier shaped the most external moraine complex at an altitude 60 m lower than that one

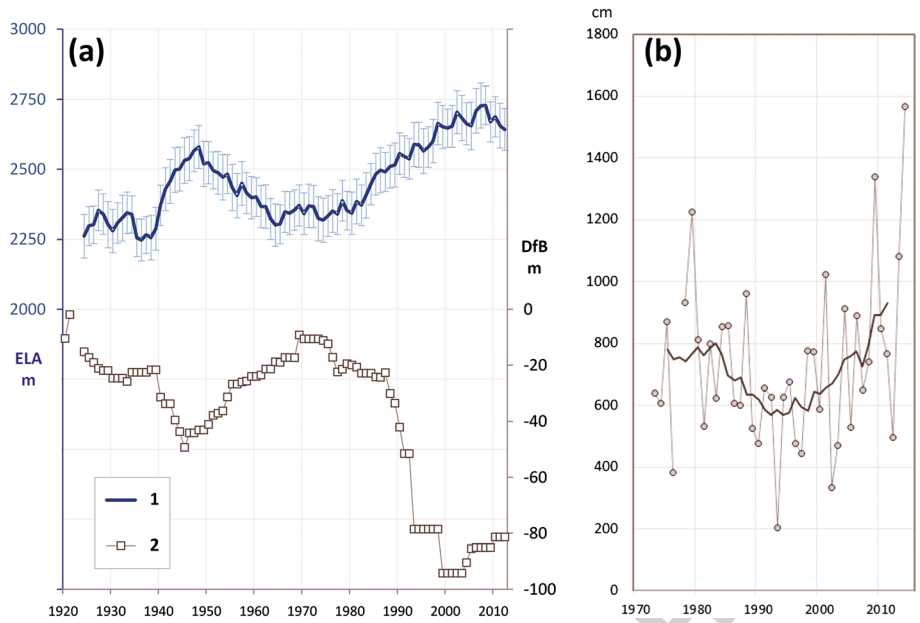

Figure 8. (a) Line 1 – equilibrium-line altitude (ELA) evolution of Canin glacier since the 1920s (11 year running mean with error bars) compared to Line 2 – the historic record of Canin eastern glacier-front variation. (b) The winter snow accumulation (C_w) (observed data and 11 year running mean) measured in the Canin area at 1800 m a.s.l. between accumulation season 1971–1972 and 2013–2014.

formed in the 1920s. Zeleni sneg-Triglav glacier was also reported to have advanced at that time, due to an increase in fall precipitation and decrease in summer temperature (Gams, 1994). The ELA remained stable until the early 1940s, then rapidly increased to about 2550 m at the beginning of the 1950s mainly because of warmer summers and dryer winters that caused a rapid glacial retreat. Recovery of the glacier occurred slowly up to the 1970s, until the1980s when the ELA decreased and stabilized at about 2350 m, mainly due to an increase in precipitation in the accumulation season and cooler summers. The dramatic rise of the ELA to 2750 m at the beginning of the 2000s was caused by dry winters in the late 1980s and the 1990s, followed by warming spring and summer temperatures. Despite the recent warming trend in air temperature, there has been a slight decreasing trend in ELA and glacier stabilization that began in the mid 2000s, due to a significant increase in winter precipitation (Figure 8).

Discussion

ELA evolution and climate

The extent of glaciers in the Julian Alps during the LIA maximum has been reconstructed as 2.350 km^2 with an estimated volume of 0.047 km^3. Without knowledge of the previously unreported ice bodies surveyed in this study, the volume estimate would be 15% lower (0.040 km^3), an error even larger than Bahr and Radić (2012 and Pfeffer *et al.* (2014 estimated. For the most part, this survey has mapped the same number of contemporary ice bodies as in the LIA, except in the Canin area. The greater number of ice bodies can be explained by the fragmentation of the Canin glacier into numerous individual features. These glacial remnants presently cover only 10% of the LIA glacier area and 16% of the 1908 area (Figures 4a and 7a). This is consistent with observations made in the Mediterranean mountains where few real glaciers survive, and many static ice-patches are what remains from the LIA (Hughes, 2014). Triglav glacier, now almost entirely melted, had the most significant recession despite being at the highest altitude. Only two small ice patches remain, each covering about 0.003 km^2 which is <2% of the LIA area (Figure 7b). Both the residual Canin and Zeleni Sneg-Triglav ice patches are located hundreds of meters away from the LIA moraines.

The LIA ELA of the Canin glacier is much lower than in the central part of the Eastern Alps (2600–3100 m; Gross *et al.*, 1977) and very close to the lowest ELA recorded in the northern fringe of the Alps in Karwendel Mountains, at about 2300 m (Kerschner and Ivy-Ochs, 2007).

The difference in ELA between Canin and Triglav, only 30 km apart, can be explained by the different MAP and energy available for melting. Precipitation in the Triglav area is about 60% of that in Canin, while MAAT is about 2 °C cooler due to the higher elevation. The calculated potential annual solar radiation values for the glaciers differed by about 7% (961.8×10^3 W m^{-2} for Triglav and 897.4×10^3 W m^{-2} for Canin). Both higher continentality, which explains the higher sensitivity of the Triglav glacier to summer temperature (Gams, 1994), and higher potential solar radiation can explain the faster and more dramatic recession of Triglav glacier compared to Canin. Canin glacier is in a more maritime environment and thus more sensitive to winter precipitation. *Scotti et al.* (2014 presented similar evidence from the central-western Alps, where a greater and more rapid post-LIA retreat occurred at glaciers in the more continental Livigno area compared to more maritime environments in the Orobie mountains. Chinn *et al.* (2005 also demonstrated the contrasting sensitivity of maritime and continental glaciers to changes in precipitation by analyzing glaciers along a transect in Norway.

The stabilization of glaciers observed in this study since the mid 2000s has also been reported from the southern central Alps. Orobie glaciers have been stable and sometimes even had positive mass balances between 2009 and 2011, despite negative mass balances across most of the European Alps (Scotti *et al.*, 2014). In southern Europe, the growth of a small maritime glacier in Montenegro in an area with estimated MAP of 2500–3000 mm, led to the development of a new moraine crest in 2006 (Hughes, 2008). This shows how glaciers can have a positive mass balance and advance despite rising temperatures if accumulation is increasing at a greater rate than the increased melting caused by higher temperatures. Nevertheless small glaciers (area < 0.1 km^2) with large inputs from

avalanches and blowing snow are very sensitive even to extreme events on an annual scale. Ice is often still in contact with the frontal moraines/pronival ridges of these small features. This is the case in the Montasio-Jof Fuart sector, the Prevala, the Velika Ponca and the Krnica. I estimated the post-LIA loss in area of Western Montasio at 29%, while the losses for Eastern and Minor Montasio are 41 and 50%, respectively. The Velika Ponca has decreased by 53%, while the Riofreddo and Prevala showed greater reductions of about 69 and 77%, respectively, still much lower values than for Canin and Triglav. This differential change has also been observed in other maritime areas of the world. For example, no considerable changes in area occurred between 1951 and 2004 at a number of small ($< 0.4\,km^2$) glaciers in sheltered sites surrounded by steep rock walls in British Columbia, Canada, while larger glaciers in the area retreated (DeBeer and Sharp, 2009). The karst topography in the Julian Alps facilitates the accumulation of thick snow in niches and hollows, promoting perennial snow and leading to permanent ice at much lower elevations than in other topographical settings.

The morainic ridges and ramparts at many of the glacierets and ice patches in the study region create a damming effect for avalanches, allowing significant snow accumulation. However, once the space behind the ridge is filled to the crest, further avalanche input flow beyond the ridge. This is a significant observation because noticeable changes in the surface area of the glacierets are only possible when climatic conditions become so favorable to cover the ridge itself leading to glacier expansion beyond it (Kuhn, 1995). Consequently, prolonged decreases in mass balance will result in large volume reduction without any noticeable reduction in area. The clast roundness of the ridges is also consistent with a dominating snow-avalanche process (Matthews *et al.*, 2011). Moreover, the ridges are generally not parallel to the cliff faces, as would be expected for a static snow-patch. This suggests the presence of dynamics in the majority of, if not all, the ice bodies.

This is supported by the presence of sub-rounded clasts in ridges dominated by angular to sub-angular clasts (e.g. Prevala, Western Montasio).

The numerous gaps and gullies observed between the pronival ramparts are associated to major avalanche routes. The occurrence of heavy rainfall and debris flow, primarily in late summer and autumn, is another important process in the destructive evolution of these ramparts. In the Montasio-Jof Fuart area and Velika Ponca, some sections of the frontal moraine/rampart have been completely washed out down valley during major rainfall events. The specific topography of the site and balance between these destructive and constructive processes, leads to the formation and preservation of such ridges (Matthews *et al.*, 2011).

Very small dynamic *firn*/ice bodies have already been observed in other areas of the Mediterranean mountains (e.g. Grunewald and Scheithauer, 2010; Hughes, 2014). In addition, Shakesby *et al.* (1999 have shown how densely packed snow, produced in maritime peri-glacial climates with heavy winter snowfall and rapid snow-firn conversion, may slide and push boulders >50 cm in size. The distances between the ridges and the talus foot slopes of >30 to 70 m are characteristic of moraines rather than protalus (pronival) ramparts (Ballantyne and Benn, 1994). Nevertheless, Ballantyne and Benn (1994 also indicate that debris may slide and roll down over the ice body reaching a ridge located beyond this limit. This suggests the potential existence of pronival moraines with morphologies influenced by moving ice, but which also receive a gravity-fed debris supply across the topographic surface of the ice body. Serrano *et al.* (2011 posit that such ice masses should be defined ice patches of nival origin, but evidence from the LIA indicates that many were active glaciers in the past, and still show signs of dynamics. Some of the ice bodies in the Julian Alps may therefore be considered using a composite conceptual model, where a combination of kataglacial and anaglacial processes are leading to the inception of nival ice patches that still have dynamics, but where the relict-ice fraction is gradually decreasing. This was recently highlighted during a repeated GPR survey conducted over the Triglav glacier. The results showed that total volume and area of the ice patch did not change significantly between 2001 and 2013, but the volume of relict ice decreased notably (Del Gobbo *et al.*, unpublished data).

The decoupling of climate and glacial evolution in the Julian Alps is evident and has been observed at other Mediterranean glaciers (Hughes, 2014). Canin and Triglav, consistent with the majority of alpine glaciers, have retreated dramatically and lost more than 90% of their areal extent since the LIA. Their snouts are presently hundreds of meters from their LIA frontal moraine complexes. However, many other permanent *firn* bodies are still in contact with their frontal, and currently active, protalus moraines.

Matthews *et al.* (2011 analyzed a subset of avalanche-derived pronival ramparts in the maritime southwest of Norway and found relatively young ages for active features, from <2900 and <1550 years BP, with the oldest examples being of Younger Dryas age (*c.* 12.9–11.7 ka BP). Matthews *et al.* (2011 concluded that these features suggest a continued development throughout the Holocene, modulated by variations in snow-avalanche frequency reflecting decadal to millennial-scale climatic variations. The similar features in the Julian Alps could thus perhaps represent a sort of 'average limit' of the glacierets partially modified in shape by *firn*/ice pushing and modulate by long-scale climate variability. This can explain their persistence at such low altitude during a warming climatic phase with high MAP and extreme events associated with elevated winter accumulation and avalanche activity. Their age could therefore date to well before the LIA.

In contrast, the larger maritime Canin and Triglav glaciers act more like larger alpine glaciers. Reconstructed MAAT in the Canin area shows an increase of 1.6 °C (0.1 °C decade^{-1}) since 1851. For melting to be balanced by present winter accumulation at the LIA ELA, a MAAT decrease of 1.7 °C would be required, which is roughly the same value. This suggests that during the LIA the drop in temperature was sufficient for glacier inception in more maritime areas of the south-eastern Alps even without a consistent increase in precipitation. This further evidence supports the idea that, in present climate conditions, the glaciers in the Julian Alps are climatically controlled mainly by precipitation, but if they were to grow larger, temperature would become increasingly important.

Conclusions

The number of permanent *firn* bodies in the Julian Alps is higher than previously reported. The glacierized area decreased from $2.350\,km^2$ during the LIA maximum to $0.358\,km^2$ in 2012. Ten previously-unreported ice patches and glacierets have been observed and described for the first time. The glacial remnants are characterized by low dynamics and persist at very low elevations. This is possible due to high precipitation rates (the highest of the Alpine chain) and feeding by avalanches and windblown snow. The behavior of these features is typical of maritime glaciers climatically-controlled mainly by precipitation, but summer and MAAT were probably also important during the LIA due to differences in geometry.

The presence of complex karst topography enhances localized snow accumulation in hollows and dolines, and is crucial to rapid glacier inception. The reconstructed LIA ELA in the Julian Alps shows a positive gradient from west to east mainly due to decreasing precipitation. The ELA of the Canin glacier during the LIA was estimated at 2275 m, much lower than in the central part of the Eastern Alps (2600–3100 m; Gross *et al*., 1977) and close to the lowest ELA recorded in the northern Alps, in Karwendel mountains (about 2300 m; Kerschner and Ivy-Ochs, 2007). Overall, the ELA and glacier evolution are decoupled from climate; this is particularly evident in the smallest avalanche-dominated ice bodies. Pronival moraines and ramparts act as a geomorphological control on the evolution of these ice masses by damming avalanches and increasing the local mass balance. Therefore, the very small ice bodies in the Julian Alps seem to persist during climate warming due to high winter precipitation and avalanche damming. Both effects, the former particularly evident in the last 10-years, are presently counteracting increasing mean summer and annual air temperature.

Acknowledgements—This research was partially supported by the University of Trieste (Italy) through the 'Finanziamento di Ateneo per progetti di ricerca scientifica, FRA-2012 and FRA 2014' Grants. The CLIMAPARKS project, Slovenia–Italy Transnational Program 2007–2013 by the European Regional Development Fund and national funds, was also important in promoting exchanges of ideas and development of facilities like the new Automatic Weather Station of Mount Canin. The Unione Meteorologica del Friuli Venezia Giulia (UMFVG) and the Civil Defense of Friuli Venezia Giulia provided LiDAR data. The V Reggimento Aviazione Casarsa 'Rigel' logistically supported the surveys with the helicopter. Valuable help during the fieldwork activities was given also by the Direzione Centrale Risorse Agricole Naturali e Forestali, by the Ente Parco Naturale Regionale delle Prealpi Giulie and by Promotur FVG. Comments of two anonymous reviewers greatly improved the quality of the paper.

References

Almasio A. 2002. Trip to the Canin glacier. *Terra Glacialis* **5**: 189–201.

Ballantyne CK, Benn DI. 1994. Glaciological constraints on Protalus Rampart development. *Permafrost and Periglacial Processes* **5**: 145–153.

Bahr DB, Pfeffer WT, Kaser G. 2015. A review of volume–area scaling of glaciers. *Reviews of Geophysics* **53**: 95–140. DOI:10.1002/2014RG000470.

Bahr DB, Radić V. 2012. Significant contribution to total mass from very small glaciers. *The Cryosphere* **6**: 763–770.

Braithwaite RJ. 2008. Temperature and precipitation climate at the equilibrium-line altitude of glaciers expressed by the degree-day factor for melting snow. *Journal of Glaciology* **54**: 437–444.

Braithwaite RJ, Müller F. 1980. On the parameterization of glacier equilibrium line altitude. *Proceedings of the Riederalp Workshop, 1978. World Glacier Inventory*; 263–271.

Brook MS, Dean JF, Keys HJR. 2011. Response of a mid-latitude cirque glacier to climate over the last two decades: Mangaehuehu Glacier, Mt Ruapehu. *Earth Surface Processes and Landforms* **36**: 1973–1980.

Carturan L, Baldassi AB, Bondesan A, Calligaro S, Carton A, Cazorzi F, Dalla Fontana G, Francese R, Guarnieri A, Milan N, Moro D, Tarolli P. 2013. Current behaviour and dynamics of the lowermost Italian glacier (Montasio Occidentale, Julian Alps). *Geografiska Annaler: Series A, Physical Geography* **95**: 79–96. DOI:10.1111/geoa.12002.

Carturan L, Baroni C, Carton A, Cazorzi F, Dalla Fontana G, Delpero C, Salvatore MC, Seppi R, Zanoner T. 2014. Reconstructing fluctuations of La Mare Glacier (eastern Italian Alps) in the Late Holocene: new evidence for a Little Ice Age maximum around 1600 ad. *Geografiska Annaler: Series A, Physical Geography* **96**: 287–306. DOI:10.1111/geoa.12048.

Chinn TJ, Winkler S, Salinger MJ, Haakensen N. 2005. Recent glacier advances in Norway and New Zealand: a comparison of their glaciological and meteorological causes. *Geografiska Annaler: Series A, Physical Geography* **87**: 141–157.

Cogley JG, Hock R, Rasmussen LA, Arendt AA, Bauder A, Braithwaite RJ, Jansson P, Kaser G, Mo¨ ller M, Nicholson L, Zemp M. 2011. Glossary of Glacier Mass Balance and Related Terms, IHP-VII Technical Documents in Hydrology No. 86, IACS Contribution No. 2. UNESCO-IHP: Paris.

Colucci RR, Fontana D, Forte E. 2014a. Characterization of two permanent ice cave deposits in the southeastern Alps (Italy) by means of Ground Penetrating Radar (GPR). *Proceedings of the VI International Workshop on Ice Caves. Idaho Falls, USA.* http://scholarcommons.usf.edu/cgi/viewcontent.cgi?article=1006&context=iwic

Colucci RR, Forte E, Boccali C, Dossi M, Lanza L, Pipan M, Guglielmin M. 2015. Evaluation of internal structure, volume and mass of glacial bodies by integrated LiDAR and ground penetrating radar (GPR) surveys: the case study of Canin Eastern Glaciere (Julian Alps, Italy). *Surveys in Geophysics* **36**(2): 231–252. DOI:10.1007/s10712-014-9311-1.

Colucci RR, Guglielmin M. 2015. Precipitation-temperature changes and evolution of a small glacier in the southeastern European Alps during the last 90 years. *International Journal of Climatology*. DOI:10.10002/joc.4172. Q10

Colucci RR, Monegato G, Žebre M. 2014b. Glacial and proglacial deposits of the Resia valley (NE Italy): new insights on the onset and decay of the last glacial maximum in the Julian Alps. *Alpine and Mediterranean Quaternary* **27**(2): 85–104.

Dahl SO, Nesje A. 1992. Paleoclimatic implications based on equilibrium-line altitude depressions of reconstructed Younger Dryas and Holocene cirque glaciers in inner Nordfjord, western Norway. *Palaeogeography, Palaeoclimatology, Palaeoecology* **94**: 87–97.

DeBeer CM, Sharp MJ. 2009. Topographic influences on recent changes of very small glaciers in the Monashee Mountains, British Columbia, Canada. *Journal of Glaciology* **55**: 691–700.

Desio A. 1927. Le variazioni dei ghiacciai del Canin nell'ultimo quarantennio. *In Alto* **39**: 1–12 (in Italian).

Djurovič P. 2012. The Debeli Namet Glacier from the second half of the 20th century to the present. *Acta Geografica Slovenica* **52**(2): 277–301. DOI:10.3986/AGS52201.

D'Orefice M, Pecci M, Smiraglia C, Ventura R. 2000. Retreat of Mediterranean glaciers since the Little Ice Age: case study of Ghiacciaio del Calderone, central Apennines, Italy. *Arctic Antarctic and Alpine Research* **32**(2): 197–201.

Fitzharris BB, Chinn TJ, Lamont GN. 1997. Glacier balance fluctuations and atmospheric circulation patterns over the Southern Alps, New Zealand. *International Journal of Climatology* **17**(7): 745–763.

Forte E, Colucci RR, Colle Fontana M, Dossi M. 2014a. 4-D quantitative GPR analyses to study the summer mass balance of a glacier: a case history. *Proceedings of the 15th International Conference on Ground Penetrating Radar – GPR2014*

Forte E, Dossi M, Pipan M, Colucci RR. 2014b. Velocity analysis from Common Offset GPR data inversion: theory and application on synthetic and real data. *Geophysical Journal International* **197**(3): 1471–1483. DOI:10.1093/gji/ggu103.

Gabrovec M, Hrvatin M, Komac B, Ortar J, Pavšek M, Topole M, Triglav Čekada M, Zorn M. 2014. Tiglavski ledenik. *Geografija Slovenije* **30**: 252.

Gabrovec M, Ortar J, Pavšek M, Zorn M, Triglav Čekada M. 2013. The Triglav glacier between 1999 and 2012. *Acta geographica Slovenica* **53**(1): 257–293.

Gams I. 1994. Changes of the Triglav glacier in the 1955–94 period in the light of climatic indicators. *Geografski zbornik* **34**: 81–117.

Gellatly AF, Smiraglia C, Grove JM, Latham R. 1994. Recent variations of Ghiacciaio del Calderone, Abruzzi, Italy. *Journal of Glaciology* **40** (136): 486–490.

González Trueba JJ, Martín Moreno R, Martínez de Pisón E, Serrano E. 2008. Little Ice Age glaciation and current glaciers in the Iberian Peninsula. *Holocene* **18**: 551–568.

Gross G, Kerschner H, Patzelt G. 1977. Methodische Untersuchungenüberdie Schneegrenze in alpinen Gletschergebieten. *Zeitschrift für Gletscherkunde und Glazialgeologie* **12**: 223–251.

Grunewald K, Scheithauer J. 2010. Europe's southernmost glaciers: response and adaptation to climate change. *Journal of Glaciology* **195**: 129–142. DOI:10.3986/AGS53202.

Grunewald K, Weber C, Scheithauer J, Haubold F. 2006. Mikrogletscher im Piringebirge (Bulgarien). *Zeitschrift für Gletscherkunde und Glazialgeologie* **39**: 99–114 (in German). Q11

Haeberli W, Bosch H, Scherler K, Østrem G, Wallén C (eds). 1989. World Glacier Inventory: Status 1988. IAHS (ICSI)/UNEP/UNESCO/ World Glacier Monitoring Service: Zurich; 458.

Hoelzle M, Haeberli W, Dischl M, Peschke W. 2003. Secular glacier mass balance derived from cumulative glacier length changes. *Global and Planetary Change* **36**: 295–306.

Hughes PD. 2007. Recent behaviour of the Debeli Namet glacier, Durmitor, Montenegro. *Earth Surface Processes and Landforms* **32**: 1593–1602.

Hughes PD. 2008. Response of a Montenegro glacier to extreme summer heatwaves in 2003 and 2007. *Geografiska Annaler* **90A**(4): 259–267.

Hughes PD. 2009. Twenty-first century glaciers and climate in the Prokletije Mountains, Albania. *Arctic Antarctic and Alpine Research* **41**: 455–459.

Hughes PD. 2010. Little Ice Age glaciers in the Balkans: low altitude glaciation enabled by cooler temperatures and local topoclimatic controls. *Earth Surface Processes and Landforms* **35**: 229–241.

Hughes PD. 2014. Little Ice Age glaciers in the Mediterranean mountains. *Mediterranée* **122**: 45–61.

Hughes PD, Woodward JC. 2009. Glacial and periglacial environments. In The Physical Geography of the Mediterranean, Woodward JC (ed). Oxford University Press: Oxford; 353–383.

Hughes PD, Woodward JC, Gibbard PL. 2006. Quaternary glacial history of the Mediterranean mountains. *Progress in Physical Geography* **30**(3): 334–364.

Hughes PD, Woodward JC, van Calsteren PC, Thomas LE. 2011. The glacial history of the Dinaric Alps, Montenegro. *Quaternary Science Reviews* **30**: 3393–3412.

Ivy-Ochs S, Kerschner H, Maisch M, Christl M, Kubik WP, Schlüchter C. 2009. Latest Pleistocene and Holocene glacier variations in the European Alps. *Quaternary Science Reviews* **28**: 2137–2149.

Kern Z, László P. 2010. Size specific steady-state accumulation-area ratio: an improvement for equilibrium-line estimation of small palaeoglaciers. *Quaternary Science Reviews* **29**: 2781–2787.

Kerschner H, Ivy-Ochs S. 2007. Palaeoclimate from glaciers: examples from the Eastern Alps during the Alpine late glacial and early Holocene. *Global and Planetary Change* **60**: 58–71. DOI:10.1016/ j.gloplacha.2006.07.034.

Kuhn M. 1995. The mass balance of very small glaciers. *Zeitschrift für Gletscherkunde und Glazialgeologie* **31**(1–2): 171–179.

Kunaver J. 1999. Geomorfološki razvoj doline krnice in njene zadnje poledenitve [Geomorphological development of the Krnica valley and its late glaciation] (in Slovenian). *Proceedings*; 63–75.

Marinelli O. 1909. Il limite climatico delle nevi nel gruppo del M. Canin (Alpi Giulie). *Zeitschrift für Gletscherkunde* **3**(5): 334–345(in Italian).

Matthews JA, Shakesby RS, Owen G, Vater AE. 2011. Pronival rampart formation in relation to snow-avalanche activity and Schmidt-hammer exposure-age dating (SHD): three case studies from southern Norway. *Geomorphology* **130**: 280–288.

Milivojevič M, Menkovič L, Čalič J. 2008. Pleistocene glacial relief of the central part of Mt. Prokletije (Albanian Alps). *Quaternary International* **190**: 112–122.

Nicolussi K, Patzelt G. 2000. Discovery of early Holocene wood and peat on the forefield of the Pasterze Glacier, Eastern Alps, Austria. *The Holocene* **10**: 191–199.

Ohmura A, Kasser P, Funk M. 1992. Climate at the equilibrium line of glaciers. *Journal of Glaciology* **38**: 397–411.

Orombelli G, Mason P. 1997. Holocene glacier fluctuations in the Italian Alpine region. *Palaoklimaforschung* **24**: 59–65.

Pecci M, D'Agata C, Smiraglia C. 2008. Ghiacciaio del Calderone (Apennines, Italy). The mass balance of a shrinking glacier. *Geografia Fisica e Dinamica Quaternaria* **31**: 55–62.

Pellitero R, Rea BR, Spagnolo M, Bakke J, Hughes P, Ivy-Ochs S, Lukas S, Ribolini A. 2015. A GIS tool for automatic calculation of glacier equilibrium-line altitudes. *Computers & Geosciences* **82**: 55–62.

Pfeffer WT, Arendt AA, Bliss A, Bolch T, Cogley JG, Gardner AS, Hagen JO, Hock R, Kaser G, Kienholz C, Miles ES, Moholdt G, Mölg N, Paul F, Radič V, Rastner P, Raup BH, Rich J, Sharp MJ. 2014. The Randolph Consortium. The Randolph Glacier Inventory: a globally complete inventory of glaciers. *Journal of Glaciology* **60**(221): 537–552. DOI:10.3189/2014JoG13J176.

Rabagliati R, Serandrei Barbero R. 1982. I ghiacciai delle Alpi Giulie dal 1920 al 1979: spostamenti delle fronti e variazioni climatiche. *Studi Trentini di Scienze Naturali, Acta Geologica* **59**: 105–126 (in Italian).

Refsnider KA, Miller GH, Hillaire-Marcel C, Fogel ML, Ghaleb B, Bowden R. 2012. Subglacial carbonates constrain basal conditions and oxygen isotopic composition of the Laurentide Ice Sheet over Arctic Canada. *Geology* **40**: 135–138.

Scotti R, Brardinoni F, Crosta GB. 2014. Post-LIA glacier changes along a latitudinal transect in the central Italian Alps. *The Cryosphere* **8**: 2235–2252. DOI:10.5194/tc-8-2235-2014.

Serandrei Barbero R, Rabagliati R, Zecchetto S. 1989. Analisi delle misure alle fronti dei ghiacciai delle Alpi Giulie e correlazioni con i dati climatici. *Geografia Fisica e Dinamica Quaternaria* **12**: 139–149 (in Italian).

Serrano E, González-Trueba JJ, Sanjosé JJ, Del Río LM. 2011. Ice patch origin, evolution and dynamics in a temperate high mountain environment: the Jou Negro, Picos de Europa (NW Spain). *Geografiska Annaler: Series A, Physical Geography* **93**: 57–70. DOI:10.1111/ j.1468-0459.2011.00006.x.

Shakesby RA, Matthews JA, McEwan LJ, Berrisford MS. 1999. Snow-push processes in pronival (protalus) rampart formation: geomorphological evidence from Smorbotn, Romsdalspane, southern Norway. *Geografiska Annaler: Series A, Physical Geography* **81**: 31–45. DOI:10.1111/j.0435-3676.1999.00047.x.

Šifrer M. 1963. Nova geomorfološka dognanja na Triglavu. Triglavski ledenik v letih 1954–1962. *Geografski zbornik* **8**: 157–210 (in Slovenian).

Šifrer M, Košir D. 1976. Nova dognanja na Triglavskem ledeniku in ledeniku pod Skuto. *Geografski zbornik* **15**: 213–269 (in Slovenian).

Styllas MN, Schimmelpfennig I, Ghilardi M, Benedetti L. 2015. Geomorphologic and paleoclimatic evidence of Holocene glaciation on Mount Olympus, Greece. *The Holocene*. DOI:10.1177/ 0959683615618259.

Tintor W. 1993. Die Kleingletscher der Julischen Alpen. *Carinthia II* **183–103**: 405–424.

Triglav Čekada M, Zorn M, Colucci RR. 2014. Changes in the area of the Canin (Italy) and Triglav glaciers (Slovenia) since 1893 based on archive images and aerial laser scanning. *Geodetski vestnik* **58** (2): 257–277.

Triglav Čekada M, Zorn M, Kaufmann V, Lieb GK. 2012. Measurements of small Alpine glaciers: examples from Slovenia and Austria. *Geodetski vestnik* **56**(3): 462–481.

Žebre M, Stepišnik U. 2015. Glaciokarst landforms and processes of the southern Dinaric Alps. *Earth Surface Processes and Landforms*. DOI:10.1002/esp.3731.

Author Query Form

Journal: Earth Surface Processes and Landforms

Article: esp_3908

Dear Author,

During the copyediting of your paper, the following queries arose. Please respond to these by annotating your proofs with the necessary changes/additions.

- If you intend to annotate your proof electronically, please refer to the E-annotation guidelines.
- If you intend to annotate your proof by means of hard-copy mark-up, please use the standard proofing marks. If manually writing corrections on your proof and returning it by fax, do not write too close to the edge of the paper. Please remember that illegible mark-ups may delay publication.

Whether you opt for hard-copy or electronic annotation of your proofs, we recommend that you provide additional clarification of answers to queries by entering your answers on the query sheet, in addition to the text mark-up.

Query No.	Query	Remark
Q1	AUTHOR: Please confirm that given names (red) and surnames/family names (green) have been identified correctly.	
Q2	AUTHOR: The citations of the figures in the first paragraph have been removed as they are just mentioned in passing and figures should appear in numerical order.	
Q3	AUTHOR: Please define 'w.e.'	
Q4	AUTHOR: Please define SFB.	
Q5	AUTHOR: Please confirm November–April.	
Q6	AUTHOR: Please provide full reference details for Bahr et al. (1997).	
Q7	AUTHOR: Figures have been renumbered or removed in places so that the figures appear in numerical order, please check. Figure 6 now Figure 3 Figure 3 now Figure 4 Figure 4 now Figure 5 Figure 5 now Figure 6	
Q8	AUTHOR: The citation "Serandrei et al., 1989" has been changed to "Serandrei Barbero et al., 1989" to match the author name/date in the reference list. Please check if the change is fine in this occurrence and modify the subsequent occurrences, if necessary.	
Q9	AUTHOR: The citation "Chynn et al. (2005)" has been changed to "Chinn et al. (2005)" to match the author name/date in the reference list. Please check if the change is fine in this occurrence and modify the subsequent occurrences, if necessary.	
Q10	AUTHOR: Please update with volume number and page rage if possible.	
Q11	AUTHOR: Please check journal title in full, or correct.	
Q12	AUTHOR: Please provide title of the conference proceedings and location.	
Q13	AUTHOR: Please provide volume number and page range if possible.	

WILEY

USING e-ANNOTATION TOOLS FOR ELECTRONIC PROOF CORRECTION

Required software to e-Annotate PDFs: Adobe Acrobat Professional or Adobe Reader (version 7.0 or above). (Note that this document uses screenshots from Adobe Reader X)
The latest version of Acrobat Reader can be downloaded for free at: http://get.adobe.com/uk/reader/

Once you have Acrobat Reader open on your computer, click on the Comment tab at the right of the toolbar:

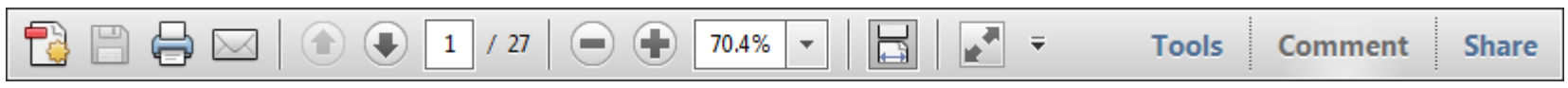

This will open up a panel down the right side of the document. The majority of tools you will use for annotating your proof will be in the Annotations section, pictured opposite. We've picked out some of these tools below:

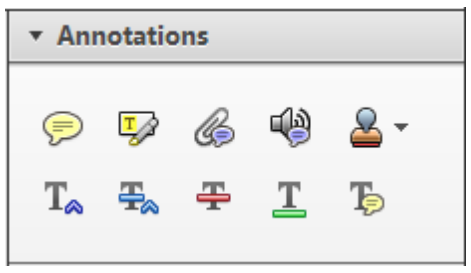

1. Replace (Ins) Tool – for replacing text.

Strikes a line through text and opens up a text box where replacement text can be entered.

How to use it

- Highlight a word or sentence.
- Click on the Replace (Ins) icon in the Annotations section.
- Type the replacement text into the blue box that appears.

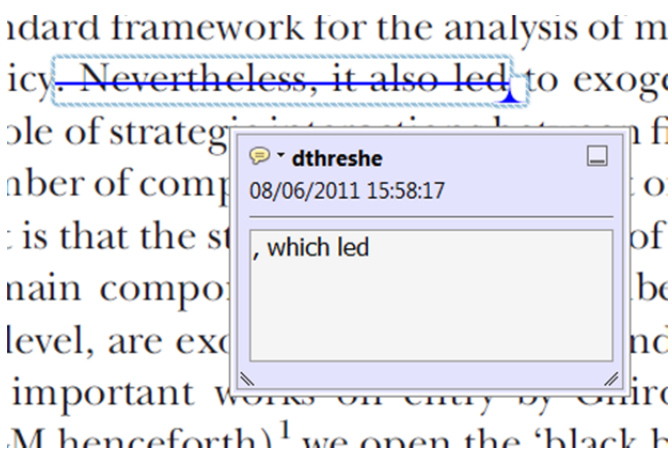

2. Strikethrough (Del) Tool – for deleting text.

Strikes a red line through text that is to be deleted.

How to use it

- Highlight a word or sentence.
- Click on the Strikethrough (Del) icon in the Annotations section.

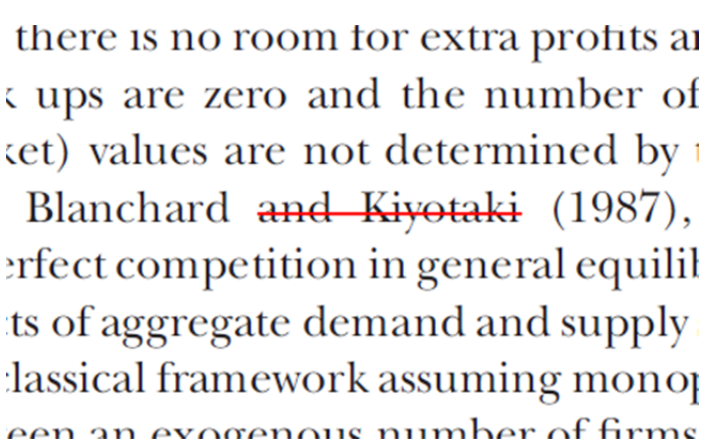

3. Add note to text Tool – for highlighting a section to be changed to bold or italic.

Highlights text in yellow and opens up a text box where comments can be entered.

How to use it

- Highlight the relevant section of text.
- Click on the Add note to text icon in the Annotations section.
- Type instruction on what should be changed regarding the text into the yellow box that appears.

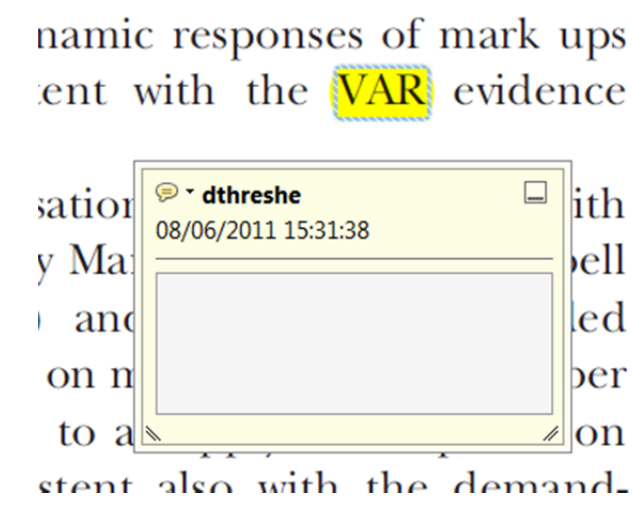

4. Add sticky note Tool – for making notes at specific points in the text.

Marks a point in the proof where a comment needs to be highlighted.

How to use it

- Click on the Add sticky note icon in the Annotations section.
- Click at the point in the proof where the comment should be inserted.
- Type the comment into the yellow box that appears.

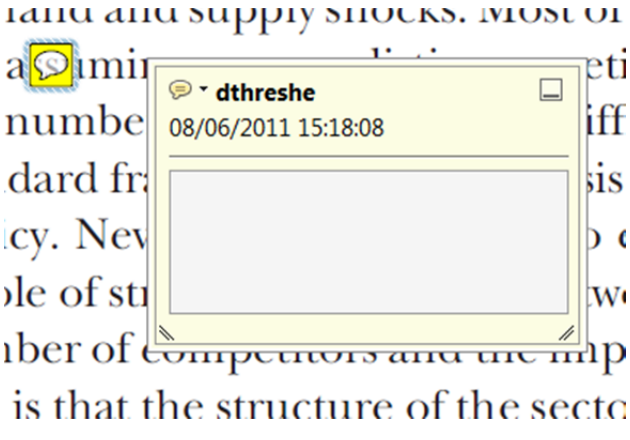

WILEY

USING e-ANNOTATION TOOLS FOR ELECTRONIC PROOF CORRECTION

5. Attach File Tool – for inserting large amounts of text or replacement figures.

Inserts an icon linking to the attached file in the appropriate pace in the text.

How to use it

- Click on the Attach File icon in the Annotations section.
- Click on the proof to where you'd like the attached file to be linked.
- Select the file to be attached from your computer or network.
- Select the colour and type of icon that will appear in the proof. Click OK.

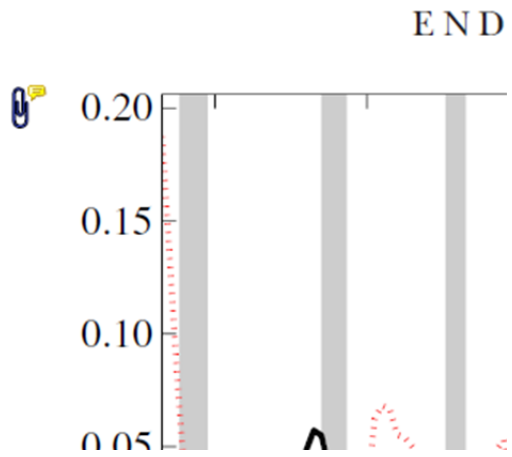

6. Add stamp Tool – for approving a proof if no corrections are required.

Inserts a selected stamp onto an appropriate place in the proof.

How to use it

- Click on the Add stamp icon in the Annotations section.
- Select the stamp you want to use. (The Approved stamp is usually available directly in the menu that appears).
- Click on the proof where you'd like the stamp to appear. (Where a proof is to be approved as it is, this would normally be on the first page).

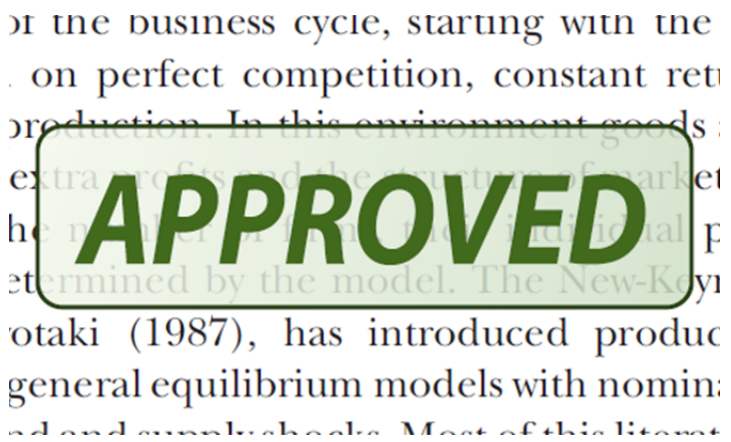

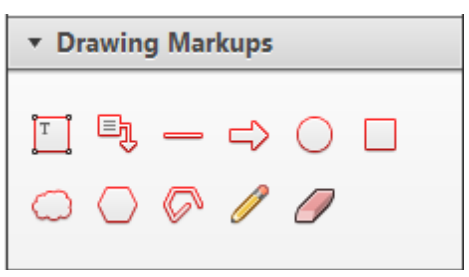

7. Drawing Markups Tools – for drawing shapes, lines and freeform annotations on proofs and commenting on these marks.

Allows shapes, lines and freeform annotations to be drawn on proofs and for comment to be made on these marks..

How to use it

- Click on one of the shapes in the Drawing Markups section.
- Click on the proof at the relevant point and draw the selected shape with the cursor.
- To add a comment to the drawn shape, move the cursor over the shape until an arrowhead appears.
- Double click on the shape and type any text in the red box that appears.

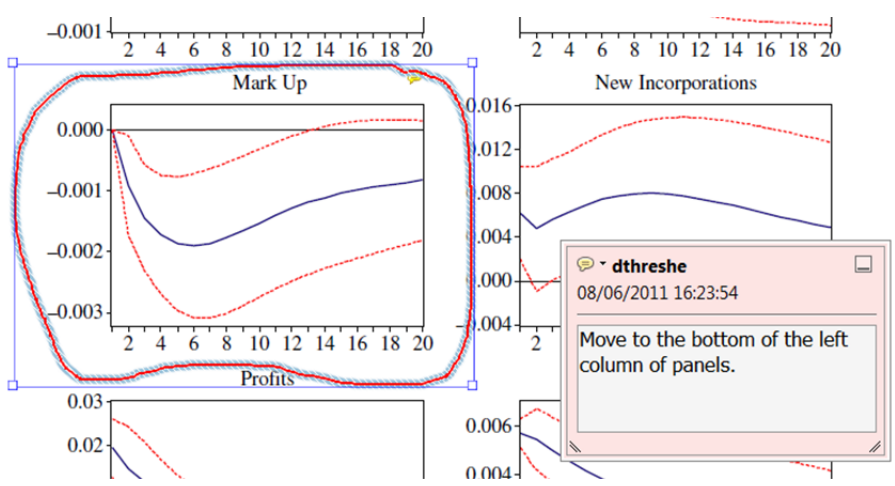

For further information on how to annotate proofs, click on the Help menu to reveal a list of further options: